

A Thermally Actuated Microelectromechanical (MEMS) Device for Measuring Viscosity

Ivan Puchades, *Member, IEEE*, and Lynn F. Fuller, *Fellow, IEEE*

Abstract—A thermally actuated non-cantilever-beam microelectromechanical viscosity sensor is presented. The proposed device is based on thermally induced vibrations of a simple silicon diaphragm and its damping due to the surrounding fluid. This vibration viscometer device utilizes thermal actuation through an *in situ* resistive heater and piezoresistive sensing, both of which utilize CMOS compatible materials leading to an inexpensive and reliable system. Thermal analysis was performed utilizing temperature diodes in the silicon diaphragm to determine the minimum heater voltage pulse amplitude and time in order to prevent heat loss to the oil under test that would lead to local viscosity changes. Viscosity measurements were performed and compared to motor oil measured on a commercial cone-and-plate viscometer. [2010-0130]

Index Terms—Membrane, microelectromechanical (MEMS), natural frequency, thermal actuation, viscosity.

I. INTRODUCTION

IN THE fields of rheology and tribology, viscosity is one of the most important factors utilized to characterize fluid properties. In the automotive industry, oil is used as an engine lubricant and it is imperative that its viscosity is kept within a specific range to provide the needed functionality. Viscosity is defined as the resistance of a fluid to flow. The higher the viscosity, the more resistance the liquid creates and the harder the engine has to work, which leads to an increase in temperature, lower fuel economy and premature engine breakdown. If the oil is too thin, it will not provide enough protection and will allow contact between the moving parts leading to engine wear out. Along with other parameters, such as acidity, water content and soot content, viscosity must be monitored as the lubricating oil degrades over its lifetime of storage or use. The main causes of this degradation are typically oxidation, hydrolysis and thermal breakdown of the organic compounds. Viscosity measurements are typically carried out with complex machines that require continuous calibration in a laboratory environment. Changes in oil viscosity in vehicles result in major breakdowns and repairs. Preventive maintenance schedules may not be enough to prevent these breakdowns. As such, in-field viscosity monitoring is needed. Microelectromechanical (MEMS) devices present an attractive solution by providing a

small, reliable and inexpensive CMOS-compatible platform in which a viscosity sensor can be made.

Current MEMS-based viscosity sensors utilize changes in resonant frequencies of cantilever beams, plates, membranes or quartz crystals to infer viscosity changes. These devices are considered vibration viscometers in which the damping of an oscillating electromechanical resonator immersed in the test liquid is measured. Complex actuation and sensing methods, which are usually non-CMOS compatible, make these devices expensive and quite challenging to fabricate and integrate. References [1]–[3] utilize an electromagnetic driven cantilever beam or plate, which require the use of a strong external magnet, and an optical readout method, both of which cannot be integrated in a low-cost CMOS platform. Reference [4] uses ZnO to achieve ultrasonic piezoelectric actuation of a very long microprobe with a piezoresistor read out. ZnO is not a standard CMOS material and the length of the vibrating microprobe raises structure reliability questions. Reference [5] also proposes the use of ZnO but in this case as a piezoelectric membrane, which improves the device reliability but not the CMOS compatibility, and requiring optical read-out. Piezoelectric quartz crystal and ZnO are respectively used by [6] and [7] to correlate changes in the transmitted surface acoustic wave frequency to density and viscosity changes.

The proposed device looks to solve the CMOS compatibility problem and to avoid the use of any external components for actuation and read out. It is based on thermally induced vibrations of a simple silicon plate and its damping due to the surrounding fluid. This MEMS viscometer would provide a device with electrical actuation and electrical output, both of which are CMOS compatible, leading to an inexpensive and reliable system.

This paper starts by reviewing the theory of thermal vibrations of plates as it applies to the proposed device. Then, theoretical and experimental analyzes are performed in order to determine the minimum amount of energy needed to actuate the device without influencing the liquid under test. The theory of fluid-plate interactions is then reviewed and compared to experimental results.

II. THERMAL VIBRATION OF PLATES

The analysis of the thermal vibrations of a plate was extensively developed around the 1950's when the aerospace industry was designing rocket-powered high-speed flight. The extremely high temperatures and temperature gradients that resulted from power generation required the analysis of the thermal stresses of the materials [8].

Manuscript received May 4, 2010; revised November 9, 2010; accepted February 23, 2011. Date of publication April 15, 2011; date of current version June 2, 2011. Subject Editor H. Seidel.

I. Puchades is with the Microsystems Engineering Department, Rochester Institute of Technology, Rochester, NY 14623 USA (e-mail: ixp6782@rit.edu).

L. F. Fuller is with the Electrical and Microelectronic Engineering Department, Rochester Institute of Technology, Rochester, NY 14623 USA (e-mail: lffeee@rit.edu).

Digital Object Identifier 10.1109/JMEMS.2011.2127447

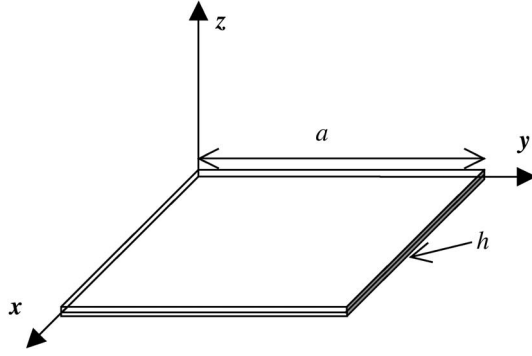


Fig. 1. Coordinate system of a thin plate or diaphragm.

The analysis of the plate illustrated in Fig. 1 is carried out below. This derivation is taken from Boley in [8]

The plate in Fig. 1 occupies the space $0 \leq x \leq a$; $0 \leq y \leq a$; $-(h/2) \leq z \leq (h/2)$. The displacements in the x , y and z directions are denoted by u , v and w , respectively. A uniform step heat input is applied at $(z = h/2)$ and results in a temperature distribution $T(z)$

$$T(z, \tau) = \frac{hQ}{k} \left[\tau + \frac{1}{2} \left(\frac{z}{h} + \frac{1}{2} \right)^2 - \frac{1}{6} - \frac{2}{\pi^2} \sum_{j=1}^{\infty} \frac{(-1)^j e^{-j^2 \pi^2 \tau}}{j^2} \cos j\pi \left(\frac{z}{h} + \frac{1}{2} \right) \right] \quad (1)$$

where Q is the applied heat. τ is a non-dimensional time parameter and is defined as the ratio of the thermal diffusivity κ , time t and the thickness of the plate h

$$\tau = \frac{\kappa t}{h^2}. \quad (2)$$

The general equation that describes the thermal vibration of plates is based on the assumption that the slopes and deflections of the plate are small when compared to any of the geometrical lengths of the plate. This assumes that the plane cross-section, which is initially perpendicular to the axis of the plate, remains plane and perpendicular to the neutral axis during bending. The fourth order differential equation that describes this motion is

$$\frac{Eh^3}{12(1-\nu^2)} \frac{\partial^4 w(x, y, t)}{\partial x^4} + \rho h \frac{\partial^2 w(x, y, t)}{\partial t^2} = -\frac{1}{1-\nu} \nabla^2 M_T \quad (3)$$

where E is the Young's modulus, ρ is the density and ν is the Poisson's ratio of the plate material.

M_T is the thermal moment and is defined as a function of τ

$$M_T = \frac{2\alpha E}{1-\nu^2} \int_{-t/2}^{t/2} Tz dz = \frac{4\alpha Q E h^3}{\pi^4 k} \left(\frac{\pi^4}{96} - \sum_{j=1,3,5}^{\infty} \frac{e^{-j^2 \pi^2 \tau}}{j^4} \right) \quad (4)$$

where α is the thermal coefficient of expansion and k is the thermal conductivity of the plate material.

TABLE I
TYPICAL PARAMETERS FOR MEMS SI SQUARE DIAPHRAGM

Material	Silicon
Density ρ	2330 kg/m ³
Young's modulus E	1.4x10 ¹¹ N/m
Poisson's ratio ν	0.3
Coefficient of thermal expansion α	2.6x10 ⁻⁶ /°C
Thermal conductivity k	150 W/m/°C
Heat capacity c_p	0.7 J/g/°C
Thermal diffusivity $\kappa = k/\rho c_p$	0.8x10 ⁻⁴ m ² /s

The solution of this equation for a simply supported plate contains static and dynamic solutions and depends on the step heat input that is applied to the plate. The solution in the vertical direction w is found to be

$$w(x, y, t) = w_{st} - w_{dyn}. \quad (5)$$

The static term w_{st} is not dependent on time and is solved by omitting the second order time derivative in (3), also called the inertia term. The inertia term can be ignored when the temperature change with time is slow enough so that this term is not significant. This is not the case in our study where the temperature is rapidly increased. The dynamic term w_{dyn} comes from the inclusion of the inertia term.

Solutions to both the static and dynamic terms are given in [8]. The dynamic solution introduces the non-dimensional parameter B as

$$B = \frac{h}{a\sqrt{\kappa}} \left(\frac{D}{h\rho} \right)^{1/4} \quad (6)$$

where

$$D = \frac{Eh^3}{12(1-\nu^2)}. \quad (7)$$

The frequency of oscillation of the diaphragm is determined by the time-dependent term, which has the form of (8). Substituting the values for B and τ , the first mode of vibration, i.e., natural frequency, $m = n = 1$, for a square diaphragm is reduced to

$$\omega_n = \frac{B^2 \pi^2 \left(m^2 + \frac{a^2}{b^2} n^2 \right) \tau}{t} = \frac{\left(\frac{h}{a\sqrt{\kappa}} \left(\frac{D}{h\rho} \right)^{1/4} \right)^2 2\pi^2 \frac{\kappa t}{h^2}}{t} = \frac{2\pi^2}{a^2} \sqrt{\frac{D}{h\rho}}. \quad (8)$$

Substituting typical values for MEMS silicon diaphragms as listed in Table I, we can calculate the natural vibration frequencies of diaphragms with $a = b = 3$ mm and $h = 10$ μ m, $h = 15$ μ m and $h = 30$ μ m. These are $f_{10\mu m} = 9750$ Hz, $f_{15\mu m} = 14626$ Hz, and $f_{30\mu m} = 29251$ Hz, respectively. The static deflection is of about 7 μ m and the amplitude of the vibration varies from about 100 nm for $h = 10$ μ m to less than 20 nm for $h = 30$ μ m. These values are similar to those measured experimentally and presented in the next sections.

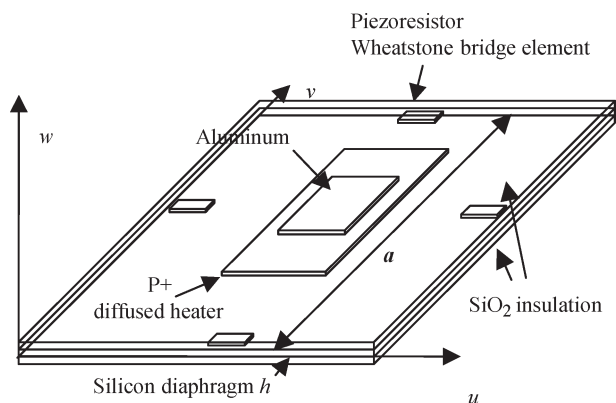


Fig. 2. Graphical representation of the thin silicon diaphragm with the P+ diffused heater actuator, the aluminum bimetal area and piezoresistor Wheatstone bridge sensing elements.

This analysis is valid as long as the structure is rapidly heated. The thermal properties of the system only affect the amplitude of the vibration and have no effect on the frequency of oscillation. As such, the rate of heating has to be faster than the characteristic thermal time, t_0 , of the structure which is defined as $t_0 = h^2/\kappa$. For our typical silicon structure with $h = 15 \mu\text{m}$, this value is $2.8 \mu\text{s}$. In addition, we use pulse heating rather than a step heat input to prevent heating of the fluid under test. This modifies Boley's theoretical model by superimposing an exponential decay at the end of the pulse. The constraints on the duration of the heating pulse are determined through analytical and experimental analysis in Section IV.

III. DESIGN AND FABRICATION

With the preceding analysis we can define the dimensions of the thermally actuated silicon resonator. In order to maximize the vertical displacement, the diaphragm thickness h should be made as small as possible and its length a should be made as large as possible. Nevertheless, these dimensions are limited. Brand *et al.* in 1994 studied the dynamic behavior of thermally actuated diaphragms and concluded that beyond a critical thickness to length ratio of 166, the amplitude of vibration and quality factor will suffer of nonlinearity, stiffening and buckling effects [9], [10]. As such, for a membrane of size $a = b = 2.5 \text{ mm}$, a thickness of $h = 15 \mu\text{m}$ is chosen. The basic configuration of the proposed MEMS viscosity sensor is presented in Fig. 2.

The realization of such a device using current microelectronic techniques leads to the use of silicon as the bulk and heater material, SiO₂ for the insulating layers, polysilicon strain gages for sensing the vertical displacement and aluminum for signal interconnections and to produce the bimetallic effect. The bimetallic effect, which is based on the difference in thermal expansion coefficient of the silicon diaphragm and the aluminum layer on top of it, is used to enhance the bowing effect of the silicon diaphragm.

A cross-section of the resulting structure is presented in Fig. 3. A p-type diffused resistor with a junction depth of approximately $5 \mu\text{m}$ is used as the thermal actuator. The membrane is designed to be square to simplify processing by

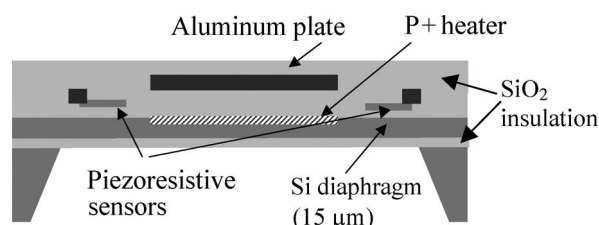


Fig. 3. Cross-sectional view of the fabricated thermal actuator with a piezoresistive polysilicon bridge and an aluminum plate for enhanced bimetal actuation.

using a well-established anisotropic KOH etch. The movement of the diaphragm is sensed with a piezoresistive bridge, which has been calibrated in [11] and results in a sensitivity of $1.35 \text{ mV}/\mu\text{m}$ when a 5 V supply is used.

A bulk MEMS microfabrication process was used to fabricate the actuator/sensor structure. The fabrication process starts with double-side-polished n-type silicon on oxide (SOI) wafers. The top silicon layer is $15 \mu\text{m}$ thick and the buried oxide is $1 \mu\text{m}$ thick. A silicon oxide is grown and used as a masking layer for the P+ spin-on-dopant process, which acts as the heating element of the membrane. After this, a pad silicon oxide is thermally grown and silicon nitride is deposited using a low-pressure chemical vapor deposition (LPCVD) process. Even though the silicon nitride and oxide are patterned on the backside of the wafer by dry SF₆ and buffered oxide etch (BOE), respectively, the diaphragms are not etched yet. Polysilicon is then deposited via LPCVD on both front and back of the wafer on top of a $0.5\text{-}\mu\text{m}$ insulating oxide layer. The polysilicon on top of the wafer is doped with phosphorous to form the Wheatstone piezoresistor sensor bridge. The polysilicon on the back of the wafer will protect the patterned nitride until the backside etch is performed at the end of the process. A $10\,000 \text{ \AA}$ low temperature oxide layer is then deposited and contact openings to poly and P+ silicon are etched out in a BOE solution. After the contacts are etched, a metal layer of $10\,000 \text{ \AA}$ of aluminum is deposited and then patterned to make the electrical connections and to act as the bimetallic layer. An additional passivation oxide of $1 \mu\text{m}$ is deposited on the front of the diaphragm in order to provide another layer of temperature isolation and prevent heat loss to the fluid under test. The front of the wafer is then protected with Brewer Science's PROTEK and the diaphragms are formed by etching from the back of the wafers. The patterned silicon nitride is used as a protection layer during the silicon KOH-etch. The $1\text{-}\mu\text{m}$ -thick buried oxide of the SOI wafers serves both as an etch-stop layer and as a thermal isolation layer on the back of the diaphragm. Fig. 3 shows a final cross-section of the fabricated device.

IV. DETERMINING PULSE DURATION

The liquid under test will affect the movement of the diaphragm by conducting the heat away. To avoid this, the heat pulse must be short enough so that the membrane temperature and movement are not influenced by the heat dissipation characteristics of the liquid [12]. Theoretically, we can get an idea of the time that it takes for a heat step input to travel through the $2.5 \mu\text{m}$ of insulation SiO₂ that is on top of the Si heater.

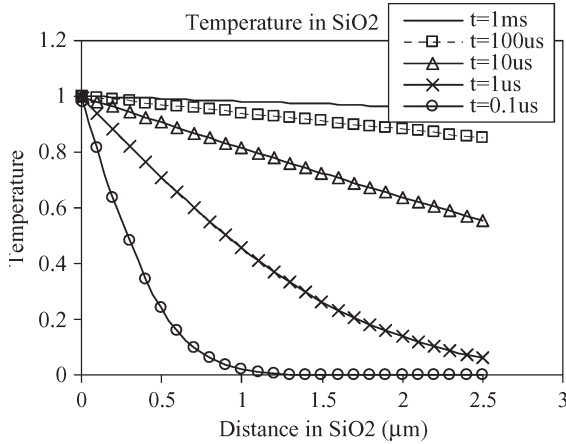


Fig. 4. Temperature distribution versus time and length for an infinitely long SiO_2 body.

Using the 1-D transient temperature equation—with $K_{\text{SiO}_2} = 0.009 \text{ cm}^2/\text{s}$ being the thermal diffusivity of SiO_2 —for a semi-infinitely long body $x \geq 0$ [12]

$$\frac{\partial T}{\partial t} = \kappa \frac{\partial^2 T}{\partial x^2}. \quad (9)$$

The solution with boundary condition of $T = T_a$ on $x = 0$ and $T = 0$ at $t = 0$ is

$$T = T_a \operatorname{erfc} \left(\frac{x}{2\sqrt{\kappa t}} \right). \quad (10)$$

The results are visualized in Fig. 4. When the time of the applied heat goes beyond $1 \mu\text{s}$ the temperature at the location $x = 2.5 \mu\text{m}$ will be influenced by the heat source. This influence will be even more significant when the time is beyond $10 \mu\text{s}$.

The analysis for the backside of the diaphragm is similar. In this case the heater is situated $15 \mu\text{m}$ away from the $1 \mu\text{m}$ SiO_2 insulating layer. As in the front of the diaphragm, pulses shorter than $10 \mu\text{s}$ should result in no significant heat loss to the surrounding media.

We determined the maximum pulse width value experimentally by monitoring the temperature of the diaphragm for pulses of different time length. The diaphragm temperature was measured using an *in situ* forward-biased PN silicon diode as a temperature sensor. The voltage drop across the forward-biased diode is temperature dependent with a negative coefficient. For a constant current bias, as temperature increases, the voltage across the diode decreases approximately $-2.2 \text{ mV}/^\circ\text{C}$.

The pulse width was reduced until the difference in diaphragm temperature when immersed in air and oil became insignificant. The pulse amplitude voltage was increased to 30 V in order to provide enough energy to the system to result in a significant diaphragm displacement. Energy is defined as the product of power and time. Thus, as we reduce pulse time, we increase the pulse power applied in order to keep a constant pulse energy input to the system.

Fig. 5 shows the measured temperature increase of the diaphragm when the sensor is placed in air (diamond symbols) and in oil (square symbols) for heat pulses of different time

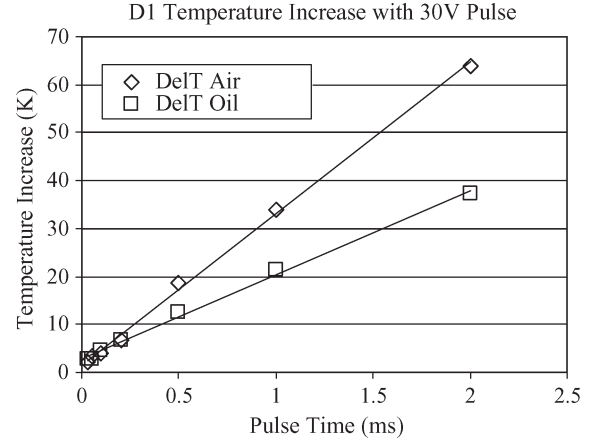


Fig. 5. Temperature increase of membrane in air and oil for pulsed heating.

duration. From Fig. 5 we observe that for a pulse of $< 0.2 \text{ ms}$ the temperature increase on the diaphragm does not seem to be influenced by the surrounding oil when compared to air. Thus, we determined that the duration of the heat pulse needed to be less than $100 \mu\text{s}$ during the operation of our devices.

V. FLUID-PLATE INTERACTIONS

The following section presents the theory of the interaction of moving plates immersed in fluids. We will use this theory to predict the behavior of our devices due to changes in density and viscosity of the fluid.

In 1920, Lamb solved the problem of a circular plate vibrating in water and found that the modes of vibrations remain approximately the same but varied in frequency by a factor called the added virtual mass β [13]. Assuming the fluid to be incompressible and inviscid, he was able to find the fluid velocity potential. By matching the plate velocity to that of the fluid at the boundary with the plate, the ratio of their kinetic energies is determined. The relation of the natural angular frequency of the plate vibrating in vacuum ω_{vacuum} and in fluid ω_{fluid} is dependent on the density of the fluid ρ_{fluid} , the plate material ρ_{plate} , and the radius a and thickness h of the circular plate as follows:

$$\omega_{\text{fluid}} = \frac{\omega_{\text{vacuum}}}{\sqrt{1 + \beta}} \quad (11)$$

where β

$$\beta = 0.669 \frac{\rho_{\text{fluid}} a}{\rho_{\text{plate}} h} \quad (12)$$

These results are based on assuming a circular plate fixed along its boundary and placed in the aperture of an infinitely rigid wall in contact with water [13]. Other authors have reported similar results [14]–[16]. The viscous effect is found to be negligible for macroscopic plates but when the thickness of the plate is reduced to the levels found of MEMS devices it must be taken into account. Ayela and Nicu observed this effect in 2007 when they reported the results of micromachined piezoelectric circular membranes vibrating in liquid media [5]. They found that Lamb's model matches well for dynamic viscosities of less than 10 centipoise (cP)—note that the viscosity of water

at room temperature is $1 \text{ cP} = 1 \times 10^{-3} \text{ Pa}\cdot\text{s}$. Beyond the 10 cP value, the shift in the natural frequency is larger than that predicted by Lamb. They also reported that the Q value of the resonance also degrades as the viscosity increases and more rapidly as the viscosity is greater than 10 cP .

Kozlovsky in 2009 picked up on Ayela and Nicu’s report and revised Lamb’s analysis to take the viscosity of the liquid into consideration as an energy dissipative element [17]. He proposed that through the “no-slip” boundary condition, the viscosity of the fluid actually couples the plate vibration to the tangential velocity of the fluid, thus increasing the fluid movement and its kinetic energy. Using a linear form of the Navier-Stokes equations he analyzed the system finding the fluid velocity, its kinetic energy and the added virtual mass taking into account the effect of the energy dissipated by viscosity.

Kozlovsky’s analysis modifies the added virtual mass factor to be

$$\beta = 0.6538 \frac{\rho_{\text{fluid}} a}{\rho_{\text{plate}} h} (1 + 1.082\xi) \quad (13)$$

where the energy dissipation of the system is characterized by ξ , which is dependent on the kinematic viscosity ν —defined as the ratio of dynamic viscosity η and density ρ —, the radial frequency of vibration ω , and the radius a of the membrane. The Q factor, which is defined as the ratio between the energy stored and dissipated per cycle, becomes

$$Q = 2\pi \frac{\text{energy_stored}}{\text{energy_dissipated_per_cycle}} \approx \frac{0.95}{\xi} \quad (14)$$

$$\xi = \sqrt{\frac{\nu}{\omega a^2}}. \quad (15)$$

Therefore, knowing both the resonance frequency and the quality factor in the liquid we can calculate the density and the viscosity of the liquid.

VI. DYNAMIC MEASUREMENTS

The natural frequency of vibration of a simply supported square thin plate can be calculated using the following well-known equation [18]:

$$f = \frac{19.74}{2\pi a^2} \left[\frac{Eh^3}{12\rho h(1-\nu^2)} \right]^{1/2} \quad (16)$$

where E is the Young’s modulus of the material, a is the length of plate, h its thickness, ρ its density and ν its Poisson’s ratio.

The typical silicon diaphragm structures used in this study have a selected diaphragm thickness of $h = 15 \mu\text{m}$ and a side length $a = 2.5 \text{ mm}$. These dimensions have been chosen to ensure linear behavior as explained in the sections above. The expected natural frequency in vacuum using the nominal values listed in Table II is $f_{\text{vacuum}} = 20604 \text{ Hz}$.

This theoretical value for the natural vibration will vary significantly due to important uncertainties found in these devices. The mechanical properties will vary due to the fact that our devices contain a $1 \mu\text{m}$ of SiO_2 for electrical and

TABLE II
NOMINAL VALUES FOR CALCULATING NATURAL FREQUENCY OF PLATE [19]

Si Young’s Modulus E	Si Poisson’s ratio ν	Si density ρ	Height of plate h	Length of plate a
190 GPa	0.3	2330 kg/m^3	$15 \times 10^{-6} \text{ m}$	$2.5 \times 10^{-3} \text{ m}$

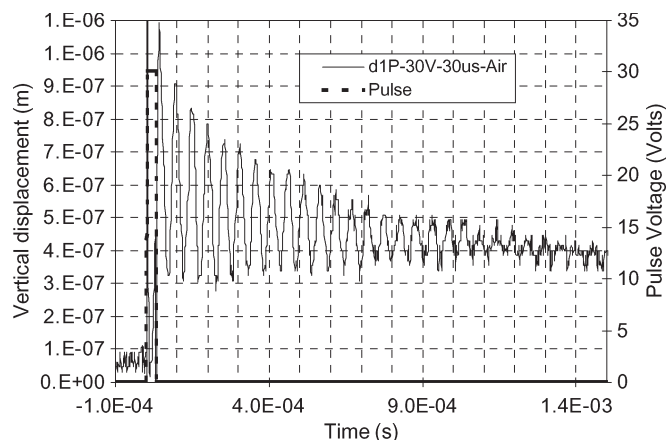


Fig. 6. Natural vibration frequency in air of device 1P with a $30 \text{ V}-30 \mu\text{s}$ pulse.

thermal isolation as well as $1\text{-}\mu\text{m}$ aluminum traces for electrical connections. Furthermore, certain degree of uncertainty already exists when using bulk material values in MEMS structures [19], [20]. There is also uncertainty of the fabricated geometrical characteristics of the device. The thickness of the plate could vary significantly since a timed etch was used to target the $15\text{-}\mu\text{m}$ thickness without the use of an etch-stop technique. This thickness could also vary across its length depending on the smoothness of the surface created by the KOH etch, which will depend on the temperature and concentration. The thickness of the plate cannot be measured without destroying the device, and even then its uniformity is difficult to measure throughout the area of the plate. The length of the plate will also vary slightly depending on the etch time and the thickness of the starting substrate. All these uncertainty leads to a range of expected values for natural frequencies. Nevertheless, finite element modal analysis confirms that (16) can be used to get a general idea of the magnitude of the expected natural vibration frequency of the structures. The experimental data shown below also supports this assertion.

Three different devices were experimentally measured. The sensors were glued and wire bonded to a PCB board with an access hole drilled on its back so that both membrane surfaces are exposed. The estimated diaphragm thickness for all three devices is of $15 \mu\text{m}$ but some variation was expected. As described in the previous sections, a $30\text{-V}-30\text{-}\mu\text{s}$ -pulse is applied to the plate heater in order to set the membrane to vibrate at its natural frequency. The deflection of the membrane is measured with the polysilicon piezoresistor Wheatstone bridge and amplified through an instrumentation amplifier. The output of device 1P is shown in Fig. 6. The vertical displacement was calculated based on the sensitivity of the Wheatstone bridge

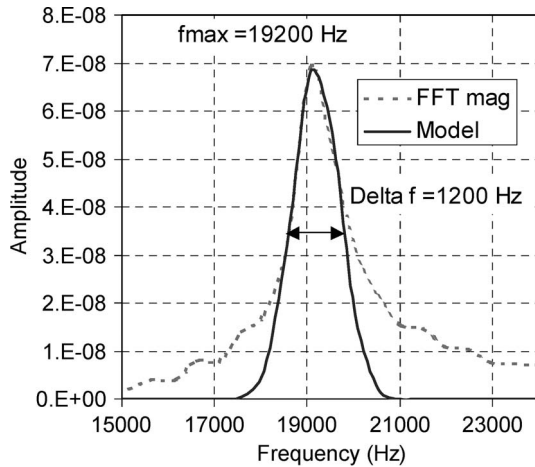


Fig. 7. FFT for device 1P. Calculating Q.

TABLE III
NATURAL FREQUENCY AND Q OF RESONATORS

Device	Natural frequency	Q	Temperature Dependence
1P	19200 Hz	16	-
25	18660 Hz	18	0.00131 Hz / Hz / °C
59	16997 Hz	15	0.00143 Hz / Hz / °C

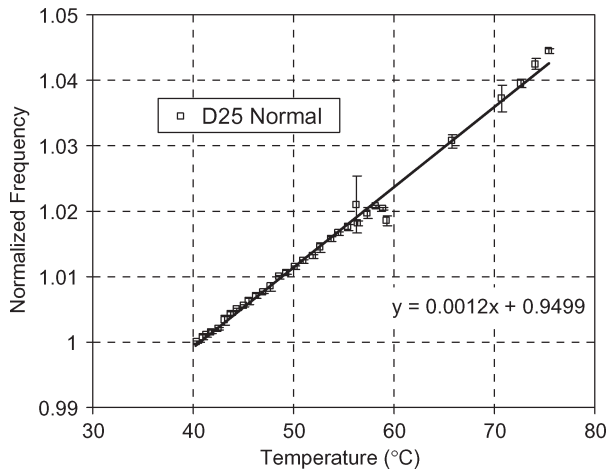


Fig. 8. Normalized frequency behavior to temperature changes of device 25 in air.

output as described in Section III. An oscilloscope was used to measure the bridge output.

A Fast Fourier Transform is performed on the signal and a normal distribution curve fitted. The natural frequency of vibration and the quality factor Q can then be extracted. Q is calculated as the ratio of the peak frequency and the width at 1/2 of maximum as shown in Fig. 7 for device 1P. The measured natural frequencies and Q-values of three different devices are presented in Table III. These values fall within the expected theoretical range.

Device 25 was further tested in air as the temperature was increased. The results shown in Fig. 8 determine that the frequency of vibration of this device increased with temperature at a rate of 0.131% / °C. Other research groups have observed this large temperature sensitivity of the vibrating natural frequency

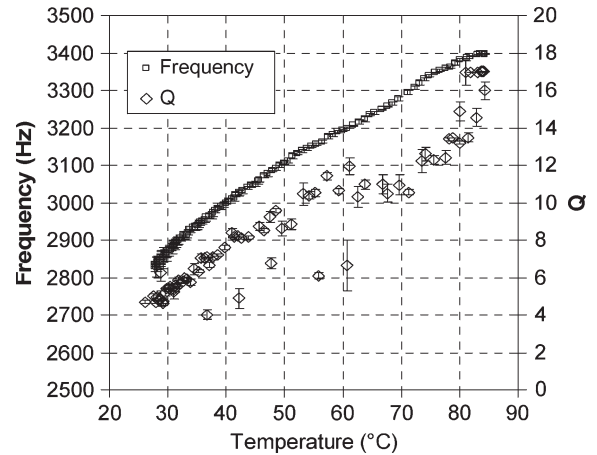


Fig. 9. Device 25. Natural frequency and Q variation versus SAE60 temperature.

during testing of packaged resonators without temperature compensation. This large temperature sensitivity is attributed to the thermal stress generated by the mismatch of thermal expansion between the device and the packaging substrate [21]. Nevertheless, the measurement error is estimated to be less than 5% for any measurement and indicates good repeatability and stability of the measurement. The measurement error was estimated by performing 10 measurements at each temperature and calculating the average and standard deviation. Error bars have been added to the measurements to indicate the expected variation. Thus, the change in natural vibration frequency of the particular sensor presented in Fig. 8 is due exclusively to the change in ambient temperature and will be used later when analyzing the sensor behavior to changes in viscosity. The Q value of the vibration did not change significantly as the temperature was increased.

VII. VISCOSITY MEASUREMENTS

Device 25 was tested in single-grade SAE60 motor oil as its viscosity was decreased by increasing its temperature. An advantage to using motor oil for this test is that it provides a non-conductive media that does not require electrical isolation of the sensor interconnects. Another advantage is that we can test a wide range of viscosities just by changing the temperature of the oil. A disadvantage is that the frequency of oscillation of the sensor will also change with temperature as measured in Section VI above. Thus, the temperature effect will need to be subtracted from the natural frequency shift to obtain an accurate measurement of viscosity.

Single grade mineral oils are generally Newtonian in behavior and their viscosity is usually not related to the shear rate. Furthermore, the rate of shear used to measure the viscosity of this fluid is kept within a narrow range for which its behavior should remain Newtonian.

The sensors were glued and wire bonded to a PCB board with an access hole drilled on its back. Thus, both surfaces of the diaphragm are in direct contact with the fluid to be tested. Fig. 9 shows the results of testing device 25 in SAE60 as the temperature is increased. The method for determining the

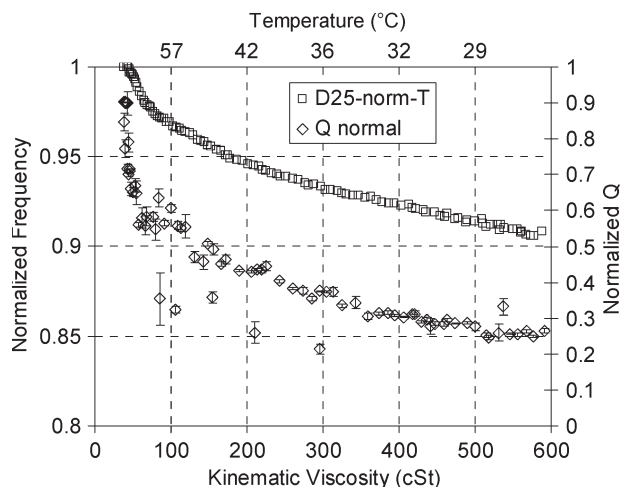


Fig. 10. Normalized frequency of vibrations and Q with respect to kinematic viscosity and temperature of the oil.

frequency of vibration and the quality factor was outlined in the previous section. The data collection method was automated through the use of National Instruments' LabView to obtain real time temperature of the oil as well as the corresponding frequency and quality factor of the vibrating sensor. Both the natural vibration frequency and Q increase as the temperature increases and the viscosity and density of the oil decrease. The estimated error for the natural vibration frequency was less than 1% of measurements at higher temperatures where the viscosity is lower and up to 5% at lower temperatures where the viscosity is higher. The error bars are barely noticeable in the frequency values in Fig 9. On the other hand, the measurements for the quality factor Q show larger variation.

During these measurements, the increase in natural vibration frequency is influenced by three factors: i) the increase in temperature, as measured in Section VI; ii) the decrease in density; and iii) the decrease in viscosity.

The effect that the temperature has on the vibration frequency can be removed based on the data presented in Section VI above. The changes in density and viscosity due to temperature can be accounted for by plotting the results versus the kinematic viscosity. The kinematic viscosity is defined as the ratio of dynamic viscosity and density and is a more appropriate metric for our sensor since the moving membrane also displaces the fluid under test. The dynamic viscosity of the SAE60 oil as a function of temperature was previously obtained using a commercial Brookfield DV-II+ Pro cone-and-plate viscometer. The change in natural vibration frequency and Q with respect to the kinematic viscosity of the oil is plotted in Fig. 10. On this plot, only the effect that the kinematic viscosity has on the natural vibration frequency and Q is shown. As expected, the natural vibration frequency decreases when the viscosity increases. The Q value also decreases but at a much larger rate.

We now compare the obtained results to both Lamb's and Kozlovsky's models in Fig. 11. Lamb's model predicted a change in vibrating frequency only due to the change in density of the fluid. This model has been verified as accurate in several studies with larger membranes and fluids of low viscosities [13]–[16]. Kozlovsky's model accounts also for changes in vis-

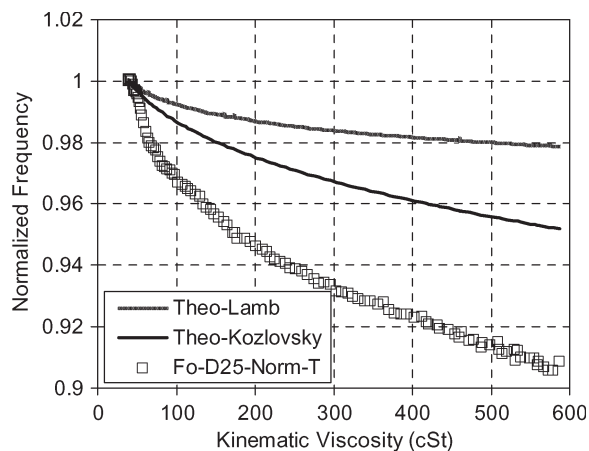


Fig. 11. Comparison of Lamb and Kozlovsky's models to experimental data.

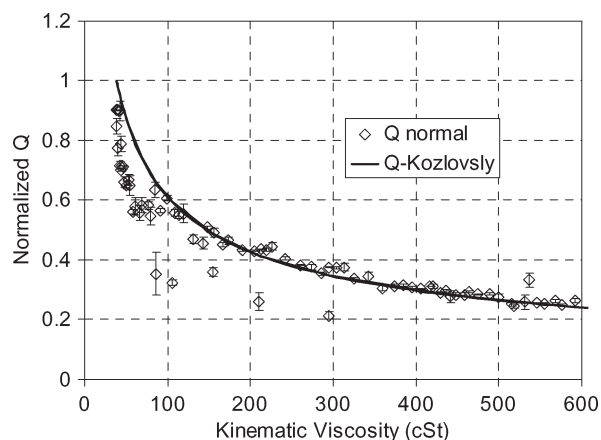


Fig. 12. Comparison of Kozlovsky model for Q-value to experimental data.

cosity. Over the range of temperatures and kinematic viscosities studied, Lamb's model predicts a change in natural vibration frequency, which is due to only the change in oil density, of approximately 2%, according to (14). Kozlovsky's model predicts a change of 5% by taking into account the viscous forces as in (15). The results show the expected general behavior described by both theoretical models. At lower viscosities the natural frequency of vibration changes more rapidly. Over 100 cSt it starts to level off. The actual results obtained indicate a change of 9%, which is larger than the predicted by either model but it leads to the conclusion that the change in density alone could not account for such a large change. It is important to remember that, for the range of values studied, the kinematic viscosity changes by over two orders of magnitude, from 40 cSt to 600 cSt. On the other hand, over this same range, the density only changes by 5%, from 833 kg / m³ to 870 kg / m³ [22].

Utilizing Kozlovsky's model as presented in (15) and (16), we can also observe the energy dissipation factor Q as a function of kinematic viscosity. Fig. 12 compares the obtained results to the predicted values. In this case, the change in Q fits the predicted values well, although it indicates a certain degree of variation especially at lower viscosities. Q decreases significantly as the viscosity of the fluid is increased. This result supports the notion that the device is actually responding to

changes in viscosity due to the fact that according to (15) the Q value would increase for increased density.

VIII. CONCLUSION

In summary, the proposed MEMS device is able to measure the viscosity variation of heated motor oil by both the change in natural vibration frequency and Q . This CMOS-compatible device has been shown to be able to operate at an elevated temperature and offers the advantage of monolithically integrating both actuation and sensing. Kozlovsky's model has been verified to correctly predict the effect of viscosity on the added virtual mass experienced on the surface of a vibrating plate immersed in fluid. Further optimization is necessary in order to produce sensors with improved sensitivities, lower power consumption and wider dynamic range. As these sensors utilize thermal actuation, it is also important to fully characterize the sensitivity, reproducibility and long-term reliability of the sensor.

REFERENCES

- [1] M. M. Lara and C. Atkinson, "Theoretical model on the interaction of a vibrating beam and the surrounding viscous fluid with applications to density and viscosity sensors," in *Proc. IEEE Sens.*, 2004, pp. 828–831.
- [2] N. Belmiloud, I. Dufour, L. Nicu, A. Colin, and J. Pistre, "Vibrating Microcantilever used as a viscometer and microrheometer," in *Proc. IEEE Sens.*, Daegu, Korea, 2006, pp. 753–756.
- [3] C. Harrison, A. Fornari, C. Hua, S. Ryu, A. R. Goodwin, K. Hsu, F. Marty, and B. Mercier, "A microfluidic MEMS sensor for the measurement of density and viscosity at high pressure," *Proc. SPIE*, vol. 6465, p. 64650U, 2007.
- [4] A. Ramkumar, X. Chen, and A. Lal, "Silicon ultrasonic horn driven microprobe viscometer," in *Proc. IEEE Ultrason. Symp.*, 2006, pp. 1449–1452.
- [5] C. Ayela and L. Nicu, "Micromachined piezoelectric membranes with high nominal quality factors in Newtonian liquid media: A Lamb's model validation at the microscale," *Sens. Actuators B, Chem.*, vol. 123, no. 2, pp. 860–868, May 2007.
- [6] I. Goubaidouline, J. Reuber, F. Merz, and D. Johannsmann, "Simultaneous determination of density and viscosity of liquids based on quartz-crystal resonators covered with nanoporous alumina," *J. Appl. Phys.*, vol. 98, no. 1, pp. 014305-1–014305-4, Jul. 2005.
- [7] B. A. Martin, "Viscosity and density sensing with ultrasonic plate waves," *Sens. Actuators A, Phys.*, vol. 22, no. 1–3, pp. 704–708, Jun. 1989.
- [8] B. Boley and J. Weiner, *Theory of Thermal Stresses*. Malabar, FL: Robert E. Kreiger Publ. Company, 1985.
- [9] O. Brand, J. M. English, S. A. Bidstrup, and M. G. Allen, "Micromachined viscosity sensor for real-time polymerization monitoring," in *Proc. Int. Conf. Solid-State Sens. Actuators*, 1997, vol. 1, pp. 121–124.
- [10] O. Brand, H. Baltes, and U. Baldeweg, "Ultrasound-transducer using membrane resonators realized with bipolar IC technology," in *Proc. IEEE Int. Workshop Micro Electro Mech. Syst.*, 1994, pp. 33–38.
- [11] I. Puchades and L. Fuller, "Design and evaluation of a MEMS bimetallic thermal actuator for viscosity measurements," in *Proc. UGIM Symp.*, 2008, pp. 93–96.
- [12] N. Noda, R. B. Hetnarski, and Y. Tnaigawa, *Thermal Stresses*. New York: Taylor & Francis, 2003.
- [13] H. Lamb, "On the vibrations of an elastic plate in contact with water," *Proc. R. Soc. Lond. A, Containing Papers Math. Phys. Character*, vol. 98, no. 690, pp. 205–216, Nov. 1920.
- [14] J. H. Powell and J. H. Roberts, "On the frequency of vibration of circular diaphragms," *Proc. Phys. Soc. Lond.*, vol. 35, pp. 170–182, 1922–1923.
- [15] Y. Kerboua, A. A. Lakis, M. Thomas, and L. Marcouiller, "Vibration analysis of rectangular plates coupled with fluid," *Appl. Math. Model.*, vol. 32, no. 12, pp. 2570–2586, Dec. 2008.
- [16] T. P. Chang and M. F. Liu, "On the natural frequency of a rectangular isotropic plate in contact with fluid," *J. Sound Vib.*, vol. 236, no. 3, pp. 547–553, Sep. 2000.
- [17] Y. Kozlovsky, "Vibration of plates in contact with viscous fluid: Extension of Lamb's model," *J. Sound Vib.*, vol. 326, no. 1/2, pp. 332–339, Sep. 2009.
- [18] R. D. Blevins, *Formulas for Natural Frequency and Mode Shape*. New York: Van Nostrand Reinhold, 1979.
- [19] K. Petersen, "Silicon as a mechanical material," *Proc. IEEE*, vol. 70, no. 5, pp. 420–457, May 1982.
- [20] J. Dolbow and M. Gosz, "Effect of out-of-plane properties of a polyimide film on the stress fields in microelectronic structures," *Mech. Mater.*, vol. 23, no. 4, pp. 311–321, Aug. 1996.
- [21] M. A. Hopcroft, "Temperature-stabilized silicon resonators for frequency references," Ph.D. dissertation, Dept. Mech. Eng., Stanford Univ., Stanford, CA, 2007.
- [22] T. Mang and W. Dresel, *Lubricants and Lubrication*, 2nd ed. Weinheim, Germany: Wiley-VCH, 2007.



Ivan Puchades (M'05) received the B.S. degree in microelectronic engineering and the M.S. degree in electrical engineering from Rochester Institute of Technology, Rochester, NY, in 1999 and 2000, respectively, where he is currently working toward the Ph.D. degree in microsystems engineering.

From 2000 to 2005, he worked as an RF Device Engineer and BiCMOS Technology Development Engineer for Freescale Semiconductor, Phoenix, AZ.



Lynn F. Fuller (M'69–SM'85–F'97) received the B.S. and M.S.E.E. degrees from Rochester Institute of Technology (RIT), Rochester, NY, in 1970 and 1973, respectively, and the Ph.D. degree in electrical engineering from SUNY Buffalo, Buffalo, NY, in 1979.

He created the Microelectronic Engineering Program at RIT, where he is the Motorola Professor of Microelectronic Engineering.